

Hysteresis and Return Point Memory in Artificial Spin Ice Systems

A. Libál¹, C. Reichhardt², and C. J. Olson Reichhardt²

¹*Faculty of Mathematics and Computer Science, Babes-Bolyai University, RO-400591 Cluj-Napoca, Romania*

²*Theoretical Division, Los Alamos National Laboratory, Los Alamos, New Mexico 87545, USA*

(Dated: June 19, 2018)

We investigate hysteresis loops and return point memory for artificial square and kagome spin ice systems by cycling an applied bias force and comparing microscopic effective spin configurations throughout the hysteresis cycle. Return point memory loss is caused by motion of individual defects in kagome ice or of grain boundaries in square ice. In successive cycles, return point memory is recovered rapidly in kagome ice. Memory is recovered more gradually in square ice due to the extended nature of the grain boundaries. Increasing the amount of quenched disorder increases the defect density but also enhances the return point memory since the defects become trapped more easily.

PACS numbers: 75.10.Hk,75.60.Jk,75.10.Nr,82.70.Dd

Frustration effects arise in many condensed and soft matter systems when geometric constraints prevent collections of interacting elements such as spins or charged particles from simultaneously minimizing all pairwise interaction energies. One of the best known frustrated systems are the spin ices [1, 2], named for their similarity to the frustrated proton ordering in water ice [3]. Spin ices have been realized in both two and three dimensions and exhibit interesting excitations such as effective magnetic monopoles [1, 4]. More recently, artificial spin ices were created with arrays of nanomagnets [5–14], colloidal particles [15, 16], or vortices in nanostructured superconductors [17]. In artificial ices, direct visualization of the microscopic effective spin configurations is possible, and system parameters such as interaction strength, doping, or the amount of quenched disorder can be controlled. Under a varying external field, changes in the microscopic configurations can be imaged and used to construct hysteresis loops [7–9, 14], as shown for kagome ice where the motion, creation, and annihilation of topological defects along the hysteresis cycle were demonstrated [7]. Memory effects are generally associated with hysteresis, and in return point memory (RPM), the system returns to the same *microscopic* configuration after completing a hysteresis loop [18–22]. Recently developed techniques show that in real magnetic materials, RPM occurs in strongly disordered samples and is absent for weak disorder [19, 20, 22]. Certain classes of $T = 0$ disordered spin systems, such as the random field Ising model [18], exhibit perfect RPM, while other systems require many loops to organize into a state with RPM [20, 21].

Artificial spin ices are an ideal system for studying RPM since they exhibit hysteresis and the microscopic states can be visualized directly. The type of topological defect that forms and its mobility varies in different ice systems, ranging from mobile monopoles [7, 9] in kagome ice to less mobile grain boundaries [6, 17] in square ice, and this could modify the RPM behavior. To quantify this, we perform numerical simulations of hystere-

sis in artificial square and kagome spin ices constructed from colloids in double-well traps with varied amounts of quenched disorder. Our model was previously shown to capture the behavior of square and kagome ices [15, 17], and the number and type of topological defects present can be controlled by changing the amount of quenched disorder [17]. We use molecular dynamics simulations to avoid the spurious loss of RPM that occurs under Monte Carlo spin flip methods [22]. Our work implies that RPM phenomena can be studied in general artificial spin systems and not just artificial spin ice systems, which would provide a new method for exploring microscopic memory effects in condensed matter systems.

Simulation— We simulate an artificial spin ice of N charged colloidal particles trapped in an array of elongated double-well pinning sites that have two states determined by which well is occupied by the colloid. The dynamics of colloid i is governed by the overdamped equation of motion $\eta(d\mathbf{R}_i/dt) = \mathbf{F}_i^{cc} + \mathbf{F}_i^s + \mathbf{F}_{\text{ext}}$, where the damping constant $\eta = 1$. The colloid-colloid interaction force has a Yukawa or screened Coulomb form, $\mathbf{F}_i^{cc} = -F_0 q^2 \sum_{i \neq j}^N \nabla_i V(R_{ij})$, with $V(R_{ij}) = (1/R_{ij}) \exp(-\kappa R_{ij}) \hat{\mathbf{r}}_{ij}$. Here $R_{ij} = |\mathbf{R}_i - \mathbf{R}_j|$, $\hat{\mathbf{r}}_{ij} = (\mathbf{R}_i - \mathbf{R}_j)/R_{ij}$, $\mathbf{R}_{i(j)}$ is the position of particle $i(j)$, $F_0 = Z^{*2}/(4\pi\epsilon\epsilon_0)$, Z^* is the unit of charge, ϵ is the solvent dielectric constant, q is the dimensionless colloid charge, $1/\kappa = 4a_0$ is the screening length, and a_0 is the unit of distance that is typically of order a micron. We neglect hydrodynamic interactions between colloids since we work in the low volume fraction limit and the colloids remain confined in the pins. The pinning force \mathbf{F}_s arises from N_p elongated traps of length $l = 1.333a_0$, width $d_p = 0.4a_0$, and depth $f_p = 100F_0$. The pin ends are parabolic confining potentials with radius $r_p = 0.2a_0$. A cylindrical force restricts motion in the direction perpendicular to the long axis of the pinning site, and a barrier in the center of the pinning site is produced by a repulsive parabolic force of height f_r that creates two energy minima on either end of the pin [15]. For square ice the

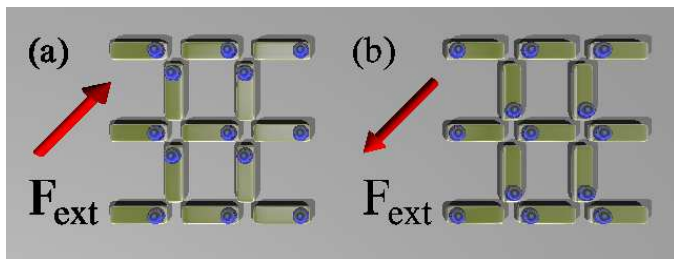


FIG. 1: Schematic of a portion of the square ice sample. A charged colloid (dots) can sit in either end of each trap (rectangles). (a) A biased state for F_{ext} applied at $\theta = 45^\circ$ from the x axis, where all the vertices are in the (0011) configuration. (b) The negative biased state after the drive is reversed contains only (1100) vertices. By cycling F_{ext} between these two extremes we construct an effective magnetization curve.

pins are arranged with $v = 4$ traps meeting at each vertex, as shown in Fig. 1, while for kagome ice, $v = 3$ traps meet at each vertex [17]. The distance between adjacent vertices is $a = 2a_0$ and there are N_v vertices. Our square ice has 35×35 vertices ($N_v = 1225$) and $N_p = 2450$ elongated pins, while our kagome ice has 40×40 vertices ($N_v = 1600$) and $N_p = 2400$ elongated pins. Disorder is added to the system by increasing or decreasing f_r in individual pinning sites according to a normal distribution with mean $f_b = 1.0F_0$ and standard deviation σ . This is analogous to varied island coercive fields in the nanomagnetic system. We initialize the system by placing a colloid in one randomly selected end of each pinning site so that $N = N_p$. To construct a hysteresis loop we apply an external force \mathbf{F}_{ext} uniformly to the sample, which for charged colloidal particles could be achieved using an external electric field. In the kagome ice $\mathbf{F}_{\text{ext}} = F_{\text{ext}}\hat{\mathbf{x}}$ while in the square ice $\mathbf{F}_{\text{ext}} = F_{\text{ext}}\sqrt{2}(\hat{\mathbf{x}} + \hat{\mathbf{y}})/2$, as shown in Fig. 1. We sweep F_{ext} from zero to a positive maximum value F_{max} , then back down through zero to a negative maximum value $-F_{\text{max}}$, and finally back up to zero to create one loop.

The vertices formed by the meeting points of the pins are categorized by $n_{in} = \sum_{i=1}^v c_i$, where $c_i = 1$ if a colloid is sitting in the end of the pin closest to the vertex and $c_i = 0$ if the colloid is sitting in the end of the pin furthest from the vertex [15, 17]. Each possible vertex type can be written as $(c_1c_2c_3c_4)$ for the square ice and as $(c_1c_2c_3)$ for the kagome ice, starting with the pinning site lying along the positive x axis with respect to the vertex and proceeding counterclockwise around the vertex. The $n_{in} = 2$ vertices in square ice do not all have the same energy. We denote the ground state vertices (1010) and (0101) as type $2gs$, and the higher energy biased vertices (1100), (0110), (0011), and (1001) as type $2b$.

We first show that our model captures the hysteretic behavior observed in artificial ice systems [7–9, 19]. In the absence of quenched disorder or drive, we find ice-

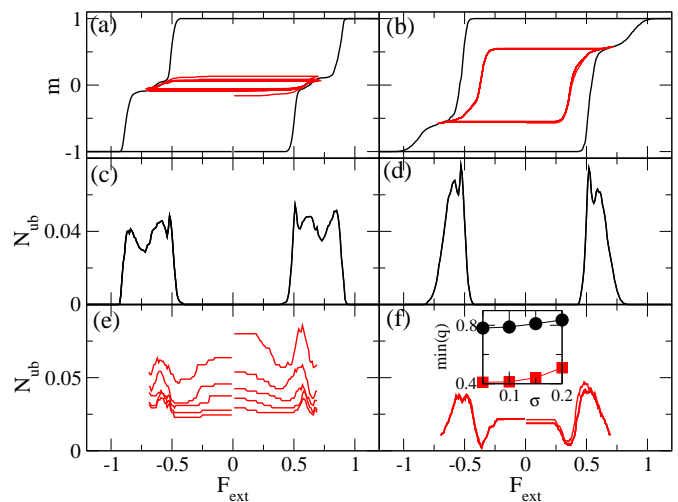


FIG. 2: (a,c,e) Square ice sample with $\sigma = 0.1$. (b,d,f) Kagome ice sample with $\sigma = 0.1$. (a,b) The reduced magnetization m vs F_{ext} . Saturation occurs at $m = \pm 1.0$ when all the vertices are in biased states. Dark line: Saturated loop with $F_{\text{max}} = 2.0$. Light lines: Consecutive loops with $F_{\text{max}} = 0.7$, below saturation. The virgin curves are not shown. (c,d) Fraction of unbiased vertices N_{ub} vs F_{ext} for the saturated loop with $F_{\text{max}} = 2.0$. (e,f) N_{ub} vs F_{ext} for repeated unsaturated loops with $F_{\text{max}} = 0.7$, with cycle number n increasing from top to bottom. For clarity, we omit the horizontal lines connecting $F_{\text{ext}} = \pm F_{\text{max}}$ to $F_{\text{ext}} = 0$. There is a much greater decrease in N_{ub} for the square ice than for the kagome ice. Inset of (f): $\min(q)$, the effective spin overlap in the $n = 2$ cycle vs σ for (circles) kagome and (squares) square ice. Samples with stronger disorder have higher q values.

rule obeying states that are ordered ground states in the square ice [15] and disordered in the kagome ice. When we add quenched disorder with $\sigma > 0$, due to its lack of extensive degeneracy the square ice forms grain boundaries composed of non-ice rule obeying vertices as shown in simulation [17] and experiment [6], while in kagome ice isolated non-ice rule defects appear [7, 17]. Under the biasing drive \mathbf{F}_{ext} shown schematically in Fig. 1(a), all the square ice vertices adopt the (0011) configuration. For kagome ice biased along the x direction, all the vertices enter the (011) state. We define the reduced magnetization m as the fraction of vertices aligned with the saturation direction, $M = N_v^{-1} \sum_{i=1}^{N_v} s_i$, where $s_i = 1$ for (0011) vertices in square ice or (011) vertices in kagome ice, $s_i = -1$ for (1100) vertices in square ice or (110) vertices in kagome ice, and $s_i = 0$ for all other vertices. In Fig. 2(a,b) we plot the hysteresis loops for square and kagome ice samples with $\sigma = 0.1$. The thick curve is obtained with $F_{\text{max}} = 2.0$, beyond the saturation level where $m = \pm 1$. We plot the fraction of unbiased vertices, $N_{ub} = N_v^{-1} \sum_{i=1}^{N_v} \delta(s_i)$, vs F_{ext} with $F_{\text{max}} = 2.0$ in Fig. 2(c,d). The completely ordered biased states are only destroyed for $0.4 < |F_{\text{ext}}| < 1.0$, close to the coercive fields at which the effective spin direction flips.

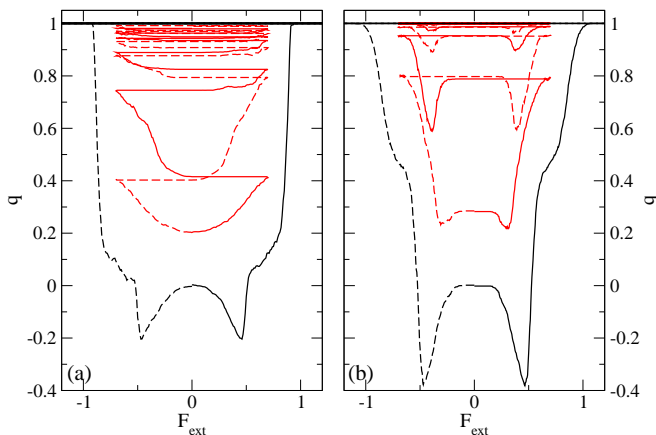


FIG. 3: Effective spin overlap q vs F_{ext} during consecutive hysteresis loops for (a) a square ice sample with $\sigma = 0.1$ and (b) a kagome ice sample with $\sigma = 0.1$. Heavy line: Saturated loops with $F_{\text{max}} = 2.0$, including the virgin curve. Thin lines: Unsaturated loops with $F_{\text{max}} = 0.7$, with n increasing from bottom to top. Solid lines: clockwise loops; dashed lines: counterclockwise loops. In the kagome ice, q approaches 1 after only a few cycles, while a much larger number of cycles are required before q approaches 1 in the square ice.

The shape of the hysteresis loop and the peaks in the non-biased defect density in Figs. 2(b,d) are in excellent agreement with the digitally constructed hysteresis loops produced in experiments on nanomagnetic kagome ice samples [7–9]. The thin lines in Figs. 2(a,b) show consecutive hysteresis loops obtained below saturation with $F_{\text{max}} = 0.7$, near the middle of the range of F_{ext} in which the largest number of defects appear. In Fig. 2(e,f) we plot N_{ub} versus F_{ext} for the unsaturated hysteresis loops. For the square ice, Fig. 2(e) shows that N_{ub} decreases with increasing n , where n is the number of loops performed, indicating that defect annihilation is occurring. For continued cycling beyond the number of loops shown in the figure, the system settles into a steady state. In the kagome ice, Fig. 2(f) shows that N_{ub} hardly changes from one cycle to the next, indicating that only a small number of defects annihilate. For the saturated case with $F_{\text{max}} = 2.0$ shown in Fig. 2(b,c), the N_{ub} curves do not evolve under repeated looping since the sample loses all memory of the microscopic configuration near the coercive field once saturation is reached.

We quantify the RPM by measuring the overlap q in the effective spin configurations along a hysteresis loop [20, 22] at equal values of F_{ext} after n complete cycles. For each trap, we define an effective spin $S_i = 1$ if the colloid is sitting in the right or top end of the trap, and $S_i = -1$ if the colloid is sitting in the left or bottom end of the trap. Writing the value of S_i after n cycles as $S_i^{(n)}$,

we measure

$$q(F_{\text{ext}}) = N^{-1} \sum_{i=1}^N S_i^{(n-1)}(F_{\text{ext}}) S_i^{(n)}(F_{\text{ext}}). \quad (1)$$

The term in the sum is 1 if the trap was biased in the same direction both before and after the complete cycle, and -1 if the colloid jumped to the other end of the trap. In Fig. 3(a,b) we plot q versus F_{ext} for both the saturated and unsaturated hysteresis curves in the square and kagome ices shown in Fig. 2(a,b). In the case of the saturated loops, q for the virgin curve in Fig. 3(a) shows that since the sample was not initialized in a biased state, the initial configuration differs significantly from the effective spin configuration obtained one cycle later, but for $n = 2$ and above, $q = 1$, indicating perfect memory. For the unsaturated loops obtained with $F_{\text{max}} = 0.7$, q is low during the first cycle, but as n increases q gradually converges to a value just below $q = 1$. A comparison with Fig. 2(e) indicates that the increase in memory with increasing n is correlated with a decrease in N_{ub} , although for this value of F_{max} there are always some defected vertices present even after the system reaches a steady state in which the grain boundaries cease to evolve. The kagome ice in Fig. 3(b) shows a similar behavior except that q approaches 1 after only a few cycles, leading to a much faster establishment of RPM than in the square ice. In Fig. 2(f) we show that the number of defected vertices remains nearly constant in the kagome ice even under repeated cycling. This indicates that although the kagome ice defects do not annihilate, they are mobile during the first few cycles and then become pinned. Our results demonstrate that for the square ice, changes in the amount of RPM are primarily associated with the annihilation of defects, while in the kagome ice, RPM is suppressed by the motion of defects.

Although the number of defects N_{ub} in both types of ice increases with increasing disorder σ , the amount of RPM increases with increasing disorder. We illustrate this in the inset of Fig. 2(f) where we plot the value of q on the $n = 2$ plateau versus σ . A similar effect was observed for real magnetic systems and in spin simulations [19, 20, 22]. In our system, q increases with increasing disorder due to the stronger pinning of the domain walls in the square ice or of the individual defects in the kagome ice. In the square ice, the disorder prevents the domain walls from coarsening. It was previously shown that as the particle-particle interaction strength in our system is reduced, non-ice-rule obeying vertices begin to appear since their energetic cost decreases [15]. For noninteracting colloids, the sample is strongly disordered but also has perfect RPM since the defected configurations are controlled only by the local disorder and are not modified by particle interactions. Thus we expect that in the experimental nanomagnetic artificial ices, when the coupling is reduced for increased spacing between the nanomagnets,

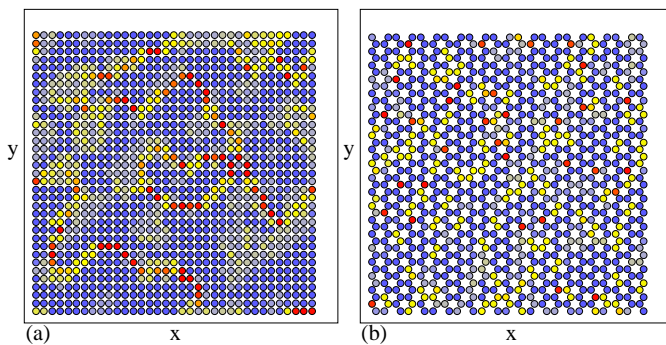


FIG. 4: Vertices in (a) square ice and (b) kagome ice samples from Fig. 2 during repeated hysteresis cycles. Vertices are colored depending on how many cycles the vertex spends in a defect state, ranging from dark blue for never defected sites to dark red for permanently defected. In (a), motion and annihilation of defects occur near grain boundaries. In (b), individual defects move and are pinned independently without forming grain boundaries.

the system should show increased or perfect RPM.

To illustrate the defect dynamics, in Fig. 4 we plot the vertices colored according to the number of hysteresis cycles each vertex spent as a defected site. Red vertices indicate locations where defects became trapped. Figure 4(a) shows that in the square ice, the defects organize into grain boundaries which move and coarsen under repeated hysteresis cycles. In Fig. 4(b), the kagome ice contains no grain boundaries but has a smaller fraction of intermediately colored vertices compared to the square ice since the isolated defects become trapped after only a few cycles. The square ice grain boundaries are less well pinned than the isolated kagome defects since they are extended objects. The motion of individual defects in kagome ice has already been imaged in experiments; it would be interesting to observe whether these defects become localized within a few hysteresis cycles.

For most artificial ice systems, thermal effects are not relevant; however, thermal fluctuations can be significant in a colloidal system. We find that our results are robust against the addition of weak thermal disorder, and that for $T > 0$ there is only a slight reduction in the asymptotic value of q and a slight increase in the number of cycles required to reach a steady state. For higher temperatures, RPM is lost even when the system is cycled to saturation since the thermal fluctuations cause random effective spin flips that change the path on each cycle. There is also no increase in RPM under repeated cycles at higher temperature [22].

In summary, we have studied hysteresis and return point memory effects for artificial square and kagome ices at the microscopic level. In the square ice for repeated unsaturated hysteresis loop cycles that extend to biases near the coercive field, the RPM increases with each cycle as the grain boundaries present in the sample coarsen

and become pinned. In kagome ice the number of defects remains nearly constant under repeated hysteresis cycles and there is much higher RPM. Here, individual defects hop rather than annihilating and are eventually pinned at sites with stronger disorder. The grain boundaries in the square ice are more mobile than the individual defects in the kagome ice since they are extended objects. Our results can be tested readily in different types of artificial ices and also could be studied in more general artificial spin systems.

This work was carried out under the auspices of the NNSA of the U.S. DoE at LANL under Contract No. DE-AC52-06NA25396.

-
- [1] R. Moessner and A.P. Ramirez, *Phys. Today* **59**(2), 24 (2006).
 - [2] A.P. Ramirez *et al.*, *Nature (London)* **399**, 333 (1999); S.T. Bramwell and M.J.P. Gingras, *Science* **294**, 1495 (2001).
 - [3] L. Pauling, *J. Am. Chem. Soc.* **57**, 2680 (1935).
 - [4] C. Castellano, R. Moessner, and S.L. Sondhi, *Nature (London)* **451**, 42 (2008); L.D.C. Jaubert and P.C.W. Holdsworth, *Nature Phys.* **5**, 258 (2009); D.J.P. Morris *et al.*, *Science* **326**, 411 (2009); S.T. Bramwell *et al.*, *Nature (London)* **461**, 956 (2009).
 - [5] R.F. Wang *et al.*, *Nature (London)* **439**, 303 (2006); G. Möller and R. Moessner, *Phys. Rev. Lett.* **96**, 237202 (2006); X. Ke *et al.*, *Phys. Rev. Lett.* **101**, 037205 (2008); C. Nisoli *et al.*, *Phys. Rev. Lett.* **105**, 047205 (2010); P.E. Lammert *et al.*, *Nature Phys.* **6**, 786 (2010); J. Li *et al.*, *Phys. Rev. B* **81**, 092406 (2010).
 - [6] J.P. Morgan, A. Stein, S. Langridge, and C.H. Marrows, *Nature Phys.* **7**, 75 (2011).
 - [7] E. Mengotti *et al.*, *Nature Phys.* **7**, 68 (2011).
 - [8] A. Schumann, B. Sothmann, P. Szary, and H. Zabel, *Appl. Phys. Lett.* **97**, 022509 (2010).
 - [9] O. Tchernyshyov, *Nature Phys.* **6**, 323 (2010); S. Ladak *et al.*, *ibid.* **6**, 359 (2010).
 - [10] Y. Qi, T. Brintlinger, and J. Cumings, *Phys. Rev. B* **77**, 094418 (2008); E. Mengotti *et al.*, *ibid.* **78**, 144402 (2008); N. Rougemaille *et al.*, *Phys. Rev. Lett.* **106**, 057209 (2011).
 - [11] M. Tanaka *et al.*, *Phys. Rev. B* **73**, 052411 (2006).
 - [12] L.A.S. Mol, W.A. Moura-Melo, and A.R. Pereira, *Phys. Rev. B* **82**, 054434 (2010).
 - [13] Z. Budrikis, P. Politi, and R.L. Stamps, *Phys. Rev. Lett.* **105**, 017201 (2010); P. Melgado, O. Petrova, Y. Shen, and O. Tchernyshyov, *Phys. Rev. Lett.* **105**, 187206 (2010).
 - [14] K.K. Kohli *et al.*, arXiv:1106.1394.
 - [15] A. Libál, C. Reichhardt, and C.J. Olson Reichhardt, *Phys. Rev. Lett.* **97**, 228302 (2006).
 - [16] Y. Han *et al.*, *Nature (London)* **456**, 898 (2008).
 - [17] A. Libál, C.J. Olson Reichhardt, and C. Reichhardt, *Phys. Rev. Lett.* **102**, 237004 (2009); Z.L. Xiao *et al.*, to be published.
 - [18] J.P. Sethna *et al.*, *Phys. Rev. Lett.* **70**, 3347 (1993).
 - [19] M.S. Pierce *et al.*, *Phys. Rev. Lett.* **94**, 017202 (2005).
 - [20] M.S. Pierce *et al.*, *Phys. Rev. B* **75**, 144406 (2007).

- [21] J.M. Deutsch and O. Narayan, Phys. Rev. Lett. **91**, 200601 (2003).
020405(R) (2006).
- [22] H.G. Katzgraber and G.T Zimanyi, Phys. Rev. B **74**,